

The effect of damage accumulation in slip bands on the resonant behavior in the very high cycle fatigue (VHCF) regime

**Philipp-Malte Hilgendorff^{1,*}, Andrei Grigorescu², Martina Zimmermann³,
Claus-Peter Fritzen¹, Hans-Jürgen Christ²**

¹ Institut für Mechanik und Regelungstechnik - Mechatronik, Universität Siegen, Siegen 57068, Germany

² Institut für Werkstofftechnik, Universität Siegen, Siegen 57068, Germany

³ Institut für Werkstoffwissenschaft, Technische Universität Dresden, Dresden 01062, Germany

* Corresponding author: philipp.hilgendorff@uni-siegen.de

Abstract

In many applications structural components are cyclically loaded up to a very high number of loading cycles due to high frequency or long product life. In this regime, particular attention is paid to the period of fatigue crack initiation and thus the localization of plastic deformation. The characterization of the damage accumulation in the VHCF regime is conducted by a new approach based on the resonant behavior of the specimen. The resonant behavior of a metastable austenitic stainless steel (AISI304) is studied experimentally in the VHCF regime and shows a distinct transient characteristic. To obtain a physically-based understanding of this characteristic, the underlying microstructural damage mechanisms and their influence on the resonant behavior are modeled. Microscopic examinations indicate that AISI304 executes localization of plastic deformation in planes/bands of intense slip. Therefore, a microstructural simulation model is proposed which accounts for the damage mechanisms of slip bands as documented by the experimental results. The model describes the behavior of slip bands taking the mechanisms of formation, sliding, slip irreversibility and cyclic hardening into account. In order to run simulations considering the real microstructure, the model is implemented into a numerical method. The two-dimensional (2-D) boundary element method is well suited for this purpose and is based on two integral equations: the displacement boundary integral equation applied to the external boundary and the stress boundary integral equation used in slip bands. Fundamental solutions within these integral equations represent anisotropic elastic behavior. By using this method, a 2-D microstructure can be reproduced that considers orientations as well as individual anisotropic elastic properties in each grain. The resonant behavior is characterized by evaluating the force-displacement hysteresis loop and using a hysteretic damping model. Results show that simulation of slip bands is in good agreement to microscopic examinations and that plastic deformation in slip bands influences the transient characteristic of the resonant behavior.

Keywords

simulation, damage accumulation, resonant behavior, boundary element method, very high cycle fatigue

1. Introduction

Observations in the regime of VHCF beyond 10 million cycles reveal that failure arises even at stress amplitudes below the conventional high cycle fatigue limit (as discussed in the series of VHCF conferences since 1998, e.g. Ref. [1]). For that reason the exploration of fatigue mechanisms in that regime and the characterization of fatigue life becomes more and more important. In the VHCF regime the period of fatigue crack initiation consumes the majority of the total fatigue life. The metastable austenitic stainless steel considered in this study conducts localization of cyclic plastic deformation by motion of dislocations which are arranged in slip bands. They are accepted as very important feature of cyclic straining in crystalline materials [2]. Slip bands are affected by cyclic slip irreversibility, which even in the VHCF regime leads to a sizeable irreversible accumulated plastic slip deformation [3].

The resonant behavior of a metastable austenitic stainless steel (AISI304) shows a distinct transient characteristic. In order to identify the microstructural damage mechanisms relevant for the transient characteristic, in the present study the damage accumulation in slip bands is modeled and its effect

on the resonant behavior is investigated. The slip band model adopted in this study is applied on a mesoscopic scale and accounts for the mechanisms of slip band formation, motion and multiplication of dislocations (expressed with the term sliding), its cyclic irreversibility and cyclic hardening.

To investigate the effect of the suggested slip band model on the resonant behavior it is adapted to the simulation of real microstructures. Several studies in the field of microstructural modeling and simulation of fatigue damage use the finite-element method (FEM) in conjunction with crystal plasticity models. Although the FE-method combined with crystal plasticity models has been devoted to a wide range of applications the implementation of the newly proposed slip band model of this study would present some difficulties: formation of new slip bands would require a remeshing algorithm and computation of sliding displacement in slip bands would necessitate special finite elements like cohesive-zone elements.

In this study a two-dimensional boundary element method (BEM) is applied, in which the proposed slip band model can be implemented very effectively. The most outstanding feature of this method is that it uses displacement differences or sliding displacements directly as unknowns on slip band layers and element discretization is confined to outer boundaries such as grain boundaries and on slip bands. The proposed BEM can simulate slip bands in a two-dimensional microstructure consisting of grains with individual anisotropic elastic properties.

In the following paragraphs at first the results of experimental examinations are given and then the simulation model with its slip band mechanisms is presented and the numerical method is specified. After presenting a procedure to determine the resonant behavior resulting from simulations, the effect of damage accumulation in slip bands on the resonant behavior is investigated in a model representing the morphology of a real microstructure.

2. Experimental Characterization

The resonant behavior of a metastable austenitic stainless steel (AISI304) is studied experimentally by means of a resonance-testing-machine, which readjusts the excitation resonant frequency during testing. The material shows a distinct transient characteristic, as shown in Fig. 1a. The lower curve in Fig. 1a indicates the test frequency at a stress amplitude of 240MPa, representing the damped resonant frequency f_{res} of the specimen-machine system. The upper curve in Fig. 1a indicates the testing frequency at low stress levels (50MPa) at distinct fatigue life stages (due to testing at 240MPa). It shows the resonance frequency f_0 of the sample without the damping effect of plastic deformation.

Fig. 1b shows a transmission electron microscopy (TEM) micrograph of the dislocation arrangement in metastable austenitic stainless steel in the fully austenitic condition fatigued under VHCF condition. The micrograph indicates that dislocations in slip bands are arranged in pile-ups at grain boundaries.

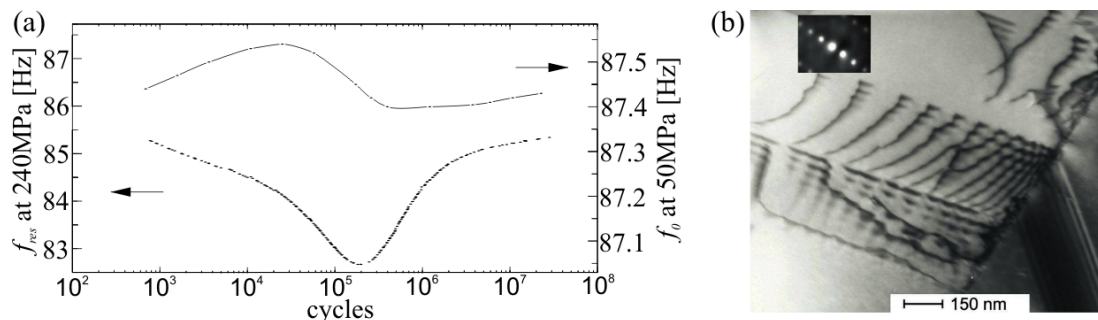


Figure 1. (a) Damped (f_{res}) and undamped (f_0) resonant frequency during cyclic loading of metastable austenitic stainless steel; (b) TEM micrograph of dislocation pile-ups at a grain boundary in metastable austenitic stainless steel (loading amplitude: 240MPa, number of cycles: 10^7)

3. Simulation Model

The plastic material behavior by localization of cyclic plastic deformation in slip bands will be considered by mechanisms which define the properties of formation, sliding, irreversibility and hardening of a slip band as follows.

Formation of a slip band is assumed to occur once a critical resolved shear stress is exceeded [4,5]. The critical resolved shear stress is defined as $\tau_{crit}^0 = 80\text{MPa}$, which corresponds to the threshold for slip band formation observed in Ref. [6].

Motivated by the TEM micrograph in Fig. 1b the model used in this study is based on the theory of dislocation pile-ups at grain boundaries [7]. Due to the equilibrium of forces produced by external loading and repulsive forces between dislocations a characteristic dislocation distribution occurs. Taking into account the distortion of a dislocation, which is defined by the magnitude of the Burgers vector, a sliding distribution $\Delta u(\xi)$ can be determined:

$$\Delta u(\xi) = \frac{2 \cdot (1-\nu)}{G} \sqrt{(l/2)^2 - \xi^2} \cdot (\tau - \tau_{crit}), \quad (1)$$

where ν and G are Poisson's ratio and shear modulus in the slip plane, respectively. l is the length of slip band and ξ is the coordinate along the slip band starting at the dislocation source. τ and τ_{crit} represent the shear stress existing in the dislocation source and the critical resolved shear stress.

It is concluded that the evolution of slip bands is related to cyclic slip irreversibility [3]. To be able to consider this mechanism in the simulation model, the slip band is approximated by two closely located layers, on which dislocation motion occurs separated in tensile and compressive loading (Fig. 2a), as Tanaka and Mura suggested in their model [8]. A special procedure was adopted to accumulate the irreversible fraction of cyclic slip. Fig. 2b shows exemplarily the variation of shear stress τ as a function of time in a slip band (in both layers) provoked by external loading and shows the resulting maximum sliding Δu^I in layer I and Δu^{II} in layer II.

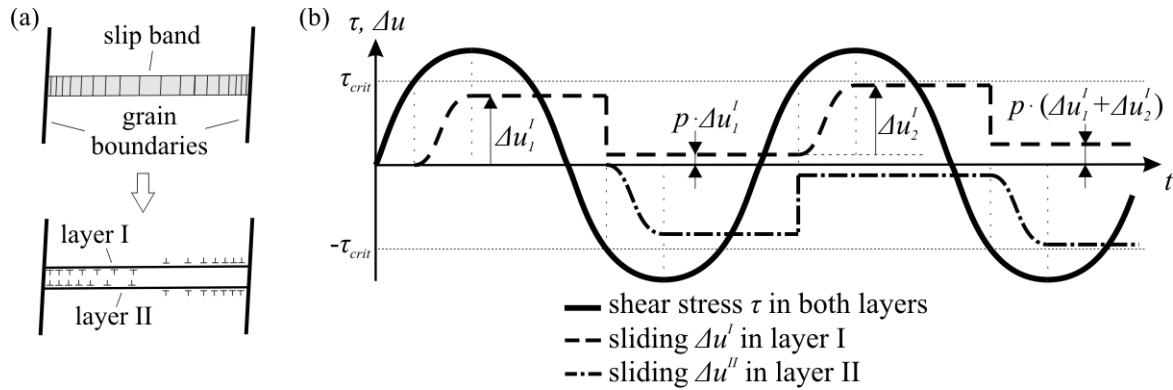


Figure 2. (a) Approximation of slip band by two closely located layers; (b) Exemplary variation of fatigue shear stress τ as a function of time in a slip band and resulting maximum sliding Δu^I in layer I and Δu^{II} in layer II

Once the critical resolved shear stress τ_{crit} in the first tensile loading is exceeded, layer I starts to slide by conducting the pile-up sliding model. As the shear stress decreases sliding is fixed at its maximum value Δu_1^I . During compressive loading layer II is activated as soon as the shear stress exceeds the critical resolved shear stress in opposite direction and concurrently in layer I, the fixed sliding Δu_1^I is reduced to an irreversible fraction $p \cdot \Delta u_1^I$. It is determined by the cyclic slip irreversibility p , which is defined as the fraction of plastic shear deformation that is irreversible in a microstructural sense [3]. One full cycle later the maximum sliding Δu_2^{II} is reduced again, but this time to an accumulated irreversible fraction denoted by the term $p \cdot (\Delta u_1^I + \Delta u_2^{II})$ taking the

irreversibility of the previous sliding into account. This procedure in combination with approximation of the slip band by two closely located layers is capable to account for irreversible fraction of sliding.

Hardening is assumed to result from a rising dislocation density. Therefore in the model the dislocation density is raised according to the plastic slip deformation in the slip band. After the slip band mechanisms are well defined in the simulation model in the following the numerical method is presented.

4. Numerical Method

The boundary element method used in this study combines the traditional displacement BEM as well as the displacement discontinuity BEM [9]. By doing so, sliding displacements can be directly evaluated in slip bands and element discretization is confined to outer boundaries such as grain boundaries and on slip bands.

The BEM used in this study is described by means of a problem statement, which consists of a two-dimensional homogeneous, anisotropic and linear elastic solid containing a finite slip line as shown in Fig. 3.

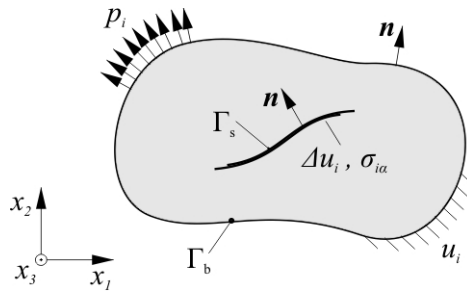


Figure 3. An anisotropic solid including a slip line

On the external boundary Γ_b displacements and tractions with components u_i and p_i are prescribed, while relative displacements Δu_i and stresses σ_{ia} are considered on one face Γ_s of the slip line. Here, relative displacements consist only of tangential relative displacements, because slip lines in contrast to cracks cannot perform opening - only sliding. Throughout the analysis the conventional summation rule over double indices is applied, Roman and Greek indices can only have the values 1 and 2. The procedure is based on two boundary integral equations: the displacement boundary integral equation, which is applied on the external boundary, and the stress boundary integral equation, which is used on the slip line face. The displacement boundary integral equation for a solid containing a slip line can be written as [9,10]:

$$c_{ij} \cdot u_i(\mathbf{x}) = \int_{\Gamma_b} [u_{ij}^*(\mathbf{x}, \mathbf{y}) \cdot p_i(\mathbf{y}) - p_{ij}^*(\mathbf{x}, \mathbf{y}) \cdot u_i(\mathbf{y})] d\Gamma_y + \int_{\Gamma_s} p_{ij}^*(\mathbf{x}, \mathbf{y}) \cdot \Delta u_i(\mathbf{y}) d\Gamma_y, \mathbf{x} \in \Gamma_b, \quad (4)$$

where c_{ij} equals 0.5 when Γ_b is smooth and $u_{ij}^*(\mathbf{x}, \mathbf{y})$ and $p_{ij}^*(\mathbf{x}, \mathbf{y})$ are the displacement and the traction fundamental solutions. Vector \mathbf{x} denotes the positions, where displacements are determined, and \mathbf{y} denotes the integration points on the boundaries Γ_b and Γ_s . The stress boundary integral equation is obtained by substituting equation (4) into Hooke's law:

$$\sigma_{j\gamma}(\mathbf{x}) = \int_{\Gamma_b} [d_{ij\gamma}^*(\mathbf{x}, \mathbf{y}) \cdot p_i(\mathbf{y}) - s_{ij\gamma}^*(\mathbf{x}, \mathbf{y}) \cdot u_i(\mathbf{y})] d\Gamma_y + \int_{\Gamma_s} s_{ij\gamma}^*(\mathbf{x}, \mathbf{y}) \cdot \Delta u_i(\mathbf{y}) d\Gamma_y, \mathbf{x} \in \Gamma_s, \quad (5)$$

where $d_{ij\gamma}^*(\mathbf{x}, \mathbf{y})$ and $s_{ij\gamma}^*(\mathbf{x}, \mathbf{y})$ are the stress and the higher-order stress fundamental solutions.

The displacement fundamental solution in equation (4) is given in Ref. [11] by Wang. He derived two-dimensional elastostatic fundamental solutions for general anisotropic solids by the use of Stroh's formalism [12]. The displacement fundamental solution in equation (4) can be given as an explicit expression:

$$u_{ij}^*(\mathbf{x}, \mathbf{y}) = \frac{1}{\pi} \text{Im} \sum_{m=1}^M \frac{A_{ij}(\eta_m)}{\partial_\eta D(\eta_m)} \log[\mathbf{d}_m \cdot (\mathbf{y} - \mathbf{x})] \quad (6)$$

with

$$A_{ij}(\eta_m) = \text{adj}[\Gamma_{ij}(1, \eta_m)], \quad (7)$$

$$D(\eta_m) = \det[\Gamma_{ij}(1, \eta_m)]. \quad (8)$$

$$\mathbf{d}_m = (1, \eta_m). \quad (9)$$

In equations (6)-(9) $\Gamma_{ij}(1, \eta_m)$ is defined by

$$\Gamma_{ij}(1, \eta_m) = C_{2ij2} \cdot \eta_m^2 + (C_{2ij1} + C_{2ji1}) \cdot \eta_m + C_{1ij1}, \quad (10)$$

where $C_{\alpha ij\beta}$ is the elasticity tensor. $D(\eta_m)$ in (6) and (8) is a polynomial function of order four and has $M=2$ complex roots η_m and two complex conjugates of η_m , which satisfy the following characteristic equation:

$$D(\eta_m) = 0. \quad (11)$$

The traction fundamental solution in equation (4) is defined by the following closed expression [10]:

$$p_{ij}^*(\mathbf{x}, \mathbf{y}) = \frac{1}{\pi} \text{Im} \sum_{m=1}^M \frac{B_{ij}(\eta_m)}{\partial_\eta D(\eta_m)} \frac{\mathbf{d}_m \cdot \mathbf{n}(\mathbf{y})}{\mathbf{d}_m \cdot (\mathbf{y} - \mathbf{x})} \quad (12)$$

with

$$B_{ij}(\eta_m) = (C_{2ip2} \cdot \eta_m + C_{2ip1}) \cdot A_{pj}(\eta_m), \quad (13)$$

and the outward unit normal vector \mathbf{n} . The stress and higher-order stress fundamental solutions in equation (5) are provided by:

$$d_{ij\gamma}^*(\mathbf{x}, \mathbf{y}) = -\frac{1}{\pi} \text{Im} \sum_{m=1}^M \frac{B_{ij\gamma}(\eta_m)}{\partial_\eta D(\eta_m)} \frac{\mathbf{d}_m}{\mathbf{d}_m \cdot (\mathbf{y} - \mathbf{x})}, \quad (14)$$

$$s_{ij\gamma}^*(\mathbf{x}, \mathbf{y}) = -\frac{1}{\pi} \text{Im} \sum_{m=1}^M \frac{C_{ij\gamma}(\eta_m)}{\partial_\eta D(\eta_m)} \frac{\mathbf{d}_m \cdot \mathbf{d}_m \cdot \mathbf{n}(\mathbf{y})}{[\mathbf{d}_m \cdot (\mathbf{y} - \mathbf{x})]^2}, \quad (15)$$

with

$$B_{ij\gamma}(\eta_m) = (C_{\gamma ip2} \cdot \eta_m + C_{\gamma ip1}) \cdot A_{pj}(\eta_m), \quad (16)$$

$$C_{ij\gamma}(\eta_m) = (C_{\gamma ip2} \cdot \eta_m + C_{\gamma ip1}) \cdot A_{pt}(\eta_m) \cdot (C_{2jt2} \cdot \eta_m + C_{2jt1}). \quad (17)$$

The integration of the fundamental solutions (6), (12), (14) and (15) are performed fully analytically. It should be noted that the solutions have a weak logarithmic singularity $\log[\mathbf{y}-\mathbf{x}]$ (6), a strong singularity $1/[\mathbf{y}-\mathbf{x}]$ (12,14), and a hypersingularity $1/[\mathbf{y}-\mathbf{x}]^2$ in the higher-order stress fundamental solution (15). For spatial discretization of equation (4) and (5) a collocation method is utilized.

In Ref. [9] and [13] a substructure technique is presented, which enables coupling of individual homogeneous substructures by use of continuity condition. The implementation of this technique in the present method allows to represent each grain by a homogeneous, elastic anisotropic substructure which is combined with other grains to a continuous microstructure.

5. Resonant behavior

The characterization of the damage accumulation in slip bands based on the resonant behavior requires a procedure to describe the resonant behavior resulting from the microstructural simulations. With the use of both the viscous and the hysteretic damping model [14] an equivalent damping ratio D and finally the resonant frequency ratio η_{res} as a describing parameter for the resonant behavior can be identified. η_{res} is basically defined as the ratio of resonant frequency of the damped system (f_{res}) and that of the undamped system (f_0). By means of energy loss per cycle ΔW , stiffness k of the specimen and displacement amplitude \hat{x} of the force displacement hysteresis loop the ratio η_{res} is given by:

$$\eta_{res} = \sqrt{1 - \frac{\Delta W^2}{2\pi^2 \cdot k^2 \cdot \hat{x}^4}} \quad (18)$$

ΔW , k and \hat{x} can be taken from the hysteresis loop, which is calculated during simulation. η_{res} can also be evaluated by using the experimental results in Fig. 1a. Thus the ratio η_{res} is applicable to compare the results from experiments with those from simulations.

In the following, the effect of damage accumulation in slip bands on the resonant behavior is investigated.

6. Simulation of damage accumulation in slip bands

The implementation of the simulation model into the BEM allows to simulate damage accumulation in slip bands in a 2-D microstructure. The investigation was carried out on the basis of the real microstructure of a metastable austenitic stainless steel characterized by means of scanning electron microscopy (SEM) in combination with the electron backscattered diffraction (EBSD)-technique and the orientation imaging microscopy (OIM) analysis.

The SEM image and EBSD map of the observed zone are shown in Fig. 4a and 4b. In addition to grain boundaries, the SEM image also highlights markings of emerging slip bands at the surface after cyclic loading. The EBSD map in Fig. 4b with related stereographic triangle indicates the crystallographic orientation of each grain.

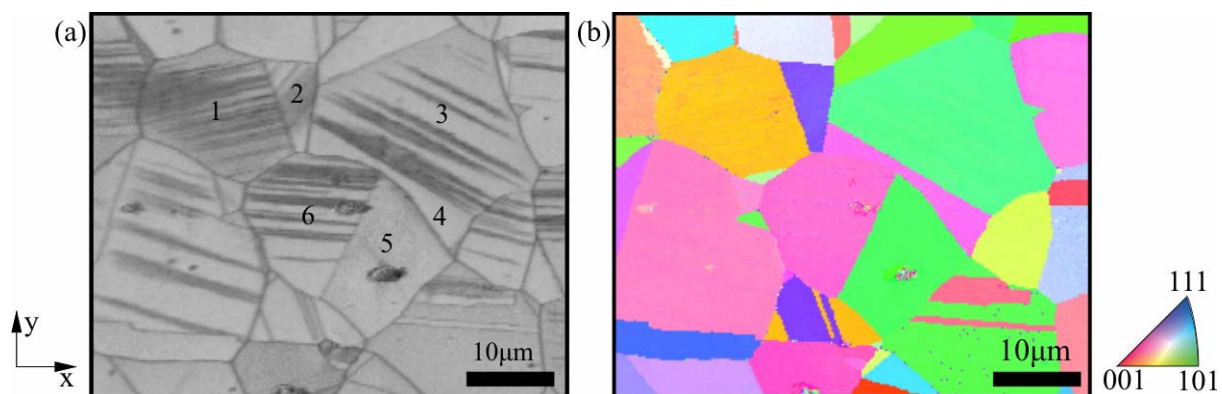


Figure 4. (a) SEM image and (b) EBSD map of the measured zone of surface grains (loading amplitude: 240MPa, number of cycles: 10^7)

In this study, primarily the contours of shear stresses in most critical slip systems are observed. For this purpose, shear stresses were computed in all of the 12 slip systems of each austenite grain and only the highest corresponding shear stresses were presented in the contours, regardless of highest Schmid factor. The elasticity tensor of the austenite phase is defined by the figures of the elastic

constants of the cubic material that are $C_{11}=205$ GPa, $C_{12}=135$ GPa and $C_{44}=125$ GPa in the present case. The 2-D BEM presupposes that exclusively in-plane sliding displacements in the x-y-plane are observed in simulations. Due to the fact, that surface roughening is strongly affected by out-of-plane sliding displacements, simulations in this study are not able to directly represent the surface roughening indicated in Fig. 4a.

Fig. 5 shows contours of simulated shear stresses in the microstructure when the simulation model is enabled. Due to the high computational effort, slip band modeling was confined to 6 grains labeled 1-6. Contours were chosen from the first, third and seventh simulated loading cycle and in each case at the maximum external loading of 240MPa. It should be noticed that one cycle in the simulation represents the microstructural damage evolution resulting from many cycles in the experiment. This was achieved by adapting the parameter of cyclic slip irreversibility p and by increasing the effect of cyclic hardening. In the simulation the cyclic slip irreversibility p is 0.2 that is much higher than usually observed for VHCF. For example in Ref. [3] a value of $p=0.000034$ for very high fatigued copper polycrystals was obtained. The effect of cyclic hardening was similarly increased in simulation.

The comparison between surface slip markings on the SEM image (Fig. 4a) and simulated slip band layers (Fig. 5) illustrates that slip bands are formed in correct slip systems. Sliding displacements in slip band layers lead to a decrease of shear stresses within grains, while at the end of slip bands significant stress peaks arise. This is particularly demonstrated in grain 4 (Fig. 5).

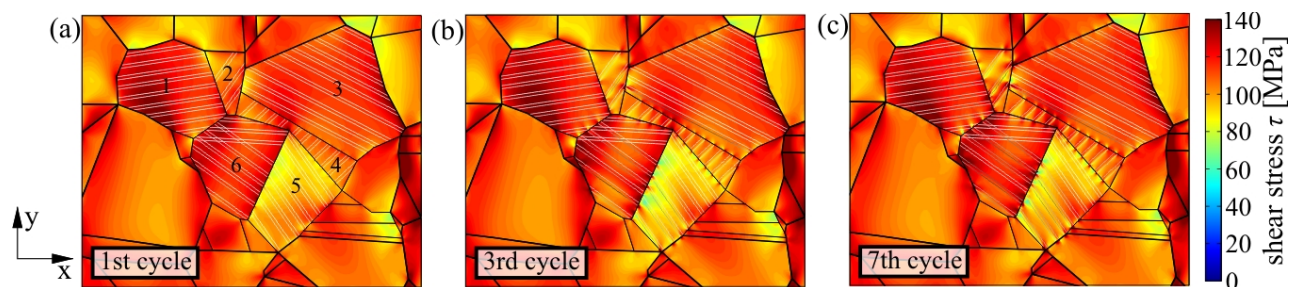


Figure 5. Contours of simulated maximum shear stresses in most critical slip systems in the 1st (a), 3rd (b) and 7th (c) loading cycle (loading amplitude: 240MPa, hypothetical cyclic slip irreversibility of $p=0.2$ (in order to represent many experimental cycles in one simulated cycle))

It is shown in Fig. 5 that slip bands deform differently depending on the specific polycrystalline boundary value problem. The comparison of contour plots in Fig. 5 in the first, third and seventh loading cycle shows that with increasing number of simulated cycles shear stresses at the end of slip bands and thus at grain boundaries increase. This is a result of the irreversible damage accumulation.

In order to investigate the effect of the microstructural damage accumulation on the resonant behavior, the force-displacement hysteresis loop is evaluated for each cycle of simulation and by using Eq. (18) the resonant frequency ratio η_{res} is determined. Fig. 6 shows the qualitative comparison of resonant frequency ratio η_{res} from simulation and experiment. Different assigning of scales for simulation (red) and experiment (black) demonstrate the qualitative manner of this comparison. A decrease of η_{res} relates to cyclic softening and an increase to cyclic strengthening.

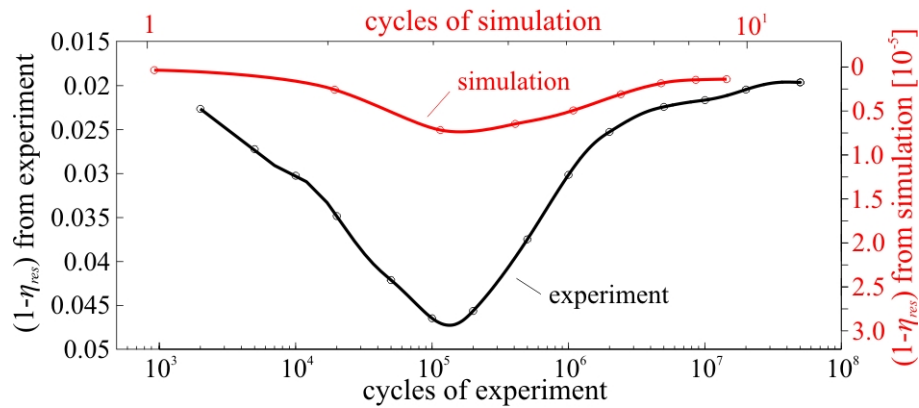


Figure 6. Qualitative comparison of resonant frequency ratio η_{res} from simulation and experiment

The results show that cyclic softening and subsequent strengthening arise from simulation of damage accumulation in slip bands. At first the mechanisms of formation and sliding cause a softening and later the mechanism of strengthening is dominating. However, by comparing the different scaling of both curves in Fig. 6 it gets obvious that the transient behavior of the experiment is much more pronounced than that of the simulation. Thus, the distinct transient characteristic of the metastable austenitic stainless steel cannot be completely reproduced by simulation of damage accumulation in slip bands. It has to be taken into account that the metastable austenitic stainless steel fulfills deformation induced martensite formation during fatigue, which might play an important role in the transient characteristic. But the mechanism of deformation induced martensite formation has not yet been considered in the model and, therefore, will be the subject of future investigations.

7. Conclusion

In this study, a simulation model is proposed that describes the damage mechanisms occurring in slip bands under VHCF condition. It is assumed that formation of a slip band occurs at sites of shear stress concentration and sliding distribution arises from the theory of dislocation pile-ups at grain boundaries. The irreversible slip character is observed as the slip band is approximated by two closely located layers and a special procedure was adopted. Hardening of the slip band results from an increasing dislocation density. The simulation model is implemented into a BEM, which is based on two boundary integral equations: the displacement boundary integral equation and the stress boundary integral equation. Fundamental solutions for general anisotropic elastic solids are used and by means of a substructure technique a 2D-microstructure with individual anisotropic elastic behavior in each grain is considered. The effect of damage accumulation in slip bands on the resonant behavior is investigated by conducting simulations in a real simulated 2-D microstructure. It turns out that slip planes of generated slip bands are in good agreement with SEM observation. The resonant behavior is characterized by the resonant frequency ratio η_{res} that can be determined from the simulated force-displacement hysteresis loop with the use of both the viscous and the hysteretic damping model. The qualitative comparison of η_{res} from simulation and experiment shows that cyclic softening and subsequent strengthening in the transient regime arise from simulation of damage accumulation in slip bands. But it becomes apparent that the variation of η_{res} from experiment is much more pronounced than that from simulation. Future work will concentrate on the effect of further microstructural inhomogeneities such as deformation induced martensite in combination with damage accumulation in slip bands.

Acknowledgements

We thank M. Wünsche for fruitful discussions regarding the boundary element method. The authors gratefully acknowledge financial support of this study by Deutsche Forschungsgemeinschaft (DFG) in the framework of the priority program Life ∞ (SPP 1466).

References

- [1] C. Berger, H.-J. Christ, Fifth international conference on very high cycle fatigue, DVM, Berlin, Germany, 2011.
- [2] J. Man, K. Obrtlík, and J. Polak, Study of surface relief evolution in fatigued 316L austenitic stainless steel by AFM, *Mat. Sci. Eng. A*, 351, (2003) 123-132.
- [3] H. Mughrabi, Cyclic slip irreversibilities and the evolution of fatigue damage, *Metall. Mater. Trans. A*, 40A, (2008) 1257-1279.
- [4] J. Yang, Y. Li, Z. Cai, S. Li, C. Ma, E. Han, W. Ke, Evolution of persistent slip bands and simulation of its stress field in a fatigued copper single crystal, *Mat. Sci. Eng. A*, 345, (2003) 164-171.
- [5] D. Zhou, J.C. Moosbrugger, D.J. Morrison, Finite element simulation of PSB macroband nucleation and propagation in single crystal nickel cycled at low plastic strain amplitudes, *Int. J. Plasticity*, 22, (2006) 1336-1366.
- [6] C. Müller-Bollenhagen, M. Zimmermann, H.-J. Christ, Adjusting the very high cycle fatigue properties of a metastable austenitic stainless steel by means of the martensite content, *Procedia Engineering*, 2, (2010) 1663-1672.
- [7] J.P. Hirth, J. Lothe, *Theory of dislocations*, 2nd ed., Krieger Publishing Company, 1992.
- [8] K. Tanaka, T. Mura, A dislocation model for fatigue crack initiation, *J. Appl. Mech.*, 48, (1981) 97-103.
- [9] M. Kübbeler, I. Roth, U. Krupp, C.-P. Fritzen, H.-J. Christ, Simulation of stage I-crack growth using a hybrid boundary element technique, *Eng. Fract. Mech.*, 78, (2011) 462-468.
- [10] M. Wünsche, Ch. Zhang, M. Kuna, S. Hirose, J. Sladek, V. Sladek, A hypersingular time-domain BEM for 2D dynamic crack analysis in anisotropic solids, *Int. J. Numer. Meth. Eng.*, 78, (2009) 127-150.
- [11] C.-Y. Wang, Two-dimensional elastostatic Green's functions for general anisotropic solids and generalization of Stroh's formalism, *Int. J. Solids Struct.*, 31, (1994) 2591-2597.
- [12] A. Stroh, Dislocations and cracks in anisotropic elasticity, *Philos. Mag.*, 3, (1958) 625-646.
- [13] M.H. Aliabadi, *The boundary element method*, Vol. 2, John Wiley and Sons, 2002.
- [14] L. Gaul, S. Bohlen, S. Kempfle, Transient and Forced Oscillations of Systems with Constant Hysteretic Damping, *Mech. Res. Comm.*, 12, (1985) 187-201.